Postprint of: Witkowski W., Rucka M., Chróścielewski J., Wilde K., On some properties of 2D spectral finite elements in problems of wave propagation, Finite Elements in Analysis and Design, Vol. 55 (2012), pp. 31-41, DOI: 10.1016/j.finel.2012.02.001

On some properties of 2D spectral finite elements in problems of wave propagation

Wojciech Witkowski*, Magdalena Rucka, Jacek Chróścielewski, Krzysztof Wilde,

Department of Structural Mechanics and Bridge Structures, Faculty of Civil and Environmental Engineering, Gdansk University of Technology, Narutowicza 11/12, 80-233, Gdańsk, Poland

*Wojciech Witkowski, wojwit@pg.gda.pl, corresponding author

Magdalena Rucka, mrucka@pg.gda.pl

Jacek Chróścielewski, jchrost@pg.gda.pl

Krzysztof Wilde, wild@pg.gda.pl

ABSTRACT. A computational analysis of plane progressive wave propagation in plane stress body is presented. The initial-boundary value problem of linear elastodynamics of Cauchy continuum is approximated spatially by specially designed multi-node C^0 displacement-based isoparametric quadrilateral spectral finite elements. To integrate element matrices the Gauss-Lobatto-Legendre quadrature rule is employed. The temporal discretization is carried out by Newmark type algorithm reformulated to accommodate the structure of local element matrices. The developed multi-node spectral elements with Gauss-Lobatto-Legendre nodes are validated by running some statics and dynamics tests to investigate the presence of locking effect and of spurious zero-energy modes. Dynamic tests, dedicated to wave propagation in L-shaped structure, are concentrated on energy propagation through right-hand angle of the construction.

Spectral finite elements, numerical simulations, wave propagation

1. Introduction

Wave propagation modelling is a subject of intensive investigations over the years. One of efficient time domain method is the spectral element method (SEM) developed by Patera [1]. The main idea of the SEM is the use of one high-order interpolating polynomial instead of low-degree polynomials usually applied in traditional FEM - finite element method (of course the FEM is not limited to low-order polynomials). Some motivation as to the use of higher-order elements in the context of wave propagation can be found for instance in [2]. The spectral finite elements are but one way of analysing wave propagation phenomena. Other possibilities are offered for example by finite difference method or by fast boundary element method. More reading on these approaches may be found for instance in [3], [4], [5].

The spectral element method has the same view point as the *p*-version of the multi-node finite element method. In the SEM approach, the Lagrange-type interpolation polynomials are applied at the Gauss-Lobbatto-Legendre (GLL) nodes, see also for instance [6]. The spectral element method can be also based on the Chebyshev polynomials as the basis functions at the

Chebyshev–Gauss–Lobatto points, see for instance [7]. The spectral elements in time domain are available for elementary structural models. The wave propagation analysis of truss and frame structures can be found in [8] and [9]. The literature on the wave propagation using SEM in two-dimensional models is limited mainly to the rectangular geometries. For example the analysis of rectangular plate structure can be found in [10] where references to other papers are given. Sridhar et al [11] developed the plane element with Chebyshev nodes to analysis of rectangular beam. Certain numerical aspects of Legendre and Chebyshev spectral elements for wave propagation in rods studied in paper [12].

The present paper is focused on the following aspects. The first one is the development of multi-node quadrilateral spectral element, its assessment and applicability to problems with some irregularities in the FEM mesh. In comparison with existing formulations, e.g. [6] where triangle elements are developed, here we present different viewpoint on the analysis of distorted elements that are necessary if irregular meshes are concerned. To modeling the complex shape elements, the quadrilateral elements undergoing mesh distortions are evaluated. In this study the particular interests is paid to the following issues associated with quadrilateral elements:

- locking effect,
- presence of spurious zero-energy modes,
- influence of mesh distortion on dispersion.

The second topic of the paper is the temporal integration scheme which is worked-out to take advantage of the diagonal structure of element matrices. Here we concentrate on preservation of the total energy of the structure during simulation time. Thirdly, having the tested 2D element we undertake numerical study of the behavior of the front of plane progressive propagating waves while travelling through joint or irregularity of the geometry. Here we focus on the L-shaped structure, the geometry of which may be regarded as rough approximation of nodal connections of planar trusses. In addition the influence of the chamfering of the right-hand angle on wave propagation is investigated. In this respect we pay attention to:

- comparing the total energy of the whole structure with the total density energies computed at representative locations or cross-sections,
- the assessment of partition of the total energy carried by wave.

2. Formulation of initial-boundary value problem

Since foundations of classical continuum mechanics are well-known, in the present section we amplify only the ingredients necessary to formulate the balance of (mechanical) energy and the principle of virtual work.

We consider an elastic body B with material points x and identify the material point x with its position $\boldsymbol{x}$ in a fixed Cartesian reference system. The boundary ∂B of B possesses two non-empty components $\partial B = \partial B_d \cup \partial B_f$ which are disjoint. Specifying for two dimensional case, let u_α, $\dot{u}_\alpha$, $\ddot{u}_\alpha$, $\varepsilon_{\alpha\beta}$, $\sigma_{\alpha\beta}$, b_α, $C_{\alpha\beta\gamma\pi}$, in this order, denote the Cartesian components of the displacement vector $\boldsymbol{u}$, the velocity vector $\dot{\boldsymbol{u}} \equiv \boldsymbol{v}$, the acceleration vector $\ddot{\boldsymbol{u}} \equiv \mathbf{a}$, the (infinitesimal) strain tensor $\boldsymbol{\varepsilon}$, the Cauchy stress tensor $\boldsymbol{\sigma}$, the body force (density) $\boldsymbol{b}$ and the

positive definite elasticity tensor (see for instance [13]) $\boldsymbol{C}$. In indicial notation used throughout, Greek subscripts take on values of the integers (1, 2) and summation over repeated subscripts is implied; subscripts preceded by a comma indicate differentiation with respect to the corresponding Cartesian coordinate. The superposed dot denotes the time derivative. The complete set of field equations of the two dimensional initial-boundary value problem of the linear elastodynamics (homogenous and isotropic) takes the form (cf. for instance [13], [14], [15])

$$\varepsilon_{\alpha\beta} = \tfrac{1}{2}(u_{\alpha,\beta} + u_{\beta,\alpha}) \equiv u_{(\alpha,\beta)} \tag{1}$$

$$\sigma_{\alpha\beta,\beta} + b_\alpha = \rho \ddot{u}_\alpha , \qquad \sigma_{\alpha\beta} = C_{\alpha\beta\gamma\pi} u_{(\gamma,\pi)} \tag{2}$$

$$C_{\alpha\beta\gamma\pi} = \bar{\lambda}\, \delta_{\alpha\beta}\delta_{\gamma\pi} + \mu(\delta_{\alpha\gamma}\delta_{\beta\pi} + \delta_{\alpha\pi}\delta_{\beta\gamma}) \tag{3}$$

Here $\rho > 0$ is mass density, $\bar{\lambda}$ and μ are material constants. When expressed in terms of Young's modulus E and Poisson's ratio ν they read

$$\bar{\lambda} = \frac{E\nu}{1-\nu^2} , \qquad \mu = \frac{E}{2(1+\nu)} \tag{4}$$

To equations $(2)_1$ we adjoin the initial boundary conditions $\boldsymbol{u}(\boldsymbol{x},0) = \boldsymbol{u}_0(\boldsymbol{x})$, $\dot{\boldsymbol{u}}(\boldsymbol{x},0) = \boldsymbol{v}_0(\boldsymbol{x})$, $\forall \boldsymbol{x} \in B$, $t = 0$ and boundary conditions $\boldsymbol{u} = \bar{\boldsymbol{u}}$ on ∂B_d , $\boldsymbol{f} = \bar{\boldsymbol{f}}$ on ∂B_f where $\boldsymbol{f}$ is the surface traction vector with components $f_\alpha = \sigma_{\beta\alpha} n_\beta$ and $\boldsymbol{n}$ denotes the outward unit normal field to ∂B_d . Possible damping effect, which is not taken into account in the present formulation, can be included as discussed in [13], see also [8].

It can be shown, cf. for instance, [16], that in two dimensional case, the velocities of plane progressive elastic waves are given by

$$c_1 = \sqrt{\frac{1}{\rho}\frac{E}{1-\nu^2}} , \qquad c_2 = \sqrt{\frac{\mu}{\rho}} \tag{5}$$

for general discussion, cf. for example [14] or [17].

Let us denote for latter reference the balance of energy

$$\underbrace{\tfrac{1}{2}\int_B m[\dot{u}_\alpha(t)]^2 dV}_{K(t)} + \underbrace{\tfrac{1}{2}\int_B u_{(\alpha,\beta)} C_{\alpha\beta\gamma\pi}\, u_{(\gamma,\pi)} dV}_{U(t)} = \underbrace{\int_0^t \left[\int_B b_\alpha \dot{u}_\alpha \mathrm{d}V + \int_{\partial B_f} f_\alpha \dot{u}_\alpha \mathrm{d}S\right] d\tau}_{G_{ext}(t)} \tag{6}$$

where $m = \int_B \rho dV$, $K(t)$ is the kinetic energy density, $U(t)$ is the elastic internal energy density and $G_{ext}(t)$ is work done by external forces at $t \in [0,T]$.

The use of the energy as the measure of the solution correctness in non-dissipative systems follows from the following facts. The total energy of the system is well defined scalar value. Once the parameters of: material, geometric and load are unambiguously defined, when the load dies out the energy should be preserved during the free motion. Thus the energy may be regarded as physical property of the system understood as the union of structure and loads. Therefore, energy is independent of time step, used temporal approximation scheme and spatial approximation (finite elements used, mesh density). Writing the energy equation (6) in the homogenous form i.e.

$$U(t)+K(t)-G_{ext}(t)=0 \tag{7}$$

furnishes the criterion of correctness of temporal integration scheme. This fact is very important since the present temporal integration algorithm is not designed to preserve energy and/or momentum of the structure, cf. for instance [18], [19], [20], [21]. Hence, the conservation of energy is studied here in the examples.

Following [22] by H^1 we designate the Sobolev space of functions that is $H^1 = H^1(B) = \{w : w \in L_2;\ w_{,x} \in L_2\}$, $L_2(B) = \left\{w : \int_B w^2 dx < \infty\right\}$. The space of kinematically admissible displacements is denoted by $S = \{\boldsymbol{u} : u_i \in H^1;\ \boldsymbol{u}(\boldsymbol{x}) = \bar{\boldsymbol{u}};\ \boldsymbol{x} \in \partial B_d\}$ and the space of kinematically admissible virtual displacements satisfying homogenous boundary conditions is given by $V = \{\boldsymbol{w} : w_i \in H^1;\ \boldsymbol{w}(\boldsymbol{x}) = \boldsymbol{0};\ \boldsymbol{x} \in \partial B_d\}$. With these definitions the weak form may be stated as follows. Given $\boldsymbol{b}$, $\boldsymbol{f}$, $\bar{\boldsymbol{u}}$, $\boldsymbol{u}_0$ and $\boldsymbol{v}_0$, find $\boldsymbol{u}(t) \in S_t$, $t \in [0,T]$, such that $\forall \boldsymbol{w} \in V$

$$\int_B \rho w_\alpha \ddot{u}_\alpha \mathrm{d}V + \int_B C_{\alpha\beta\gamma\pi} w_{(\alpha,\beta)} u_{(\gamma,\pi)} \mathrm{d}V = \int_B w_\alpha b_\alpha \,\mathrm{d}V + \int_{\partial B_f} w_\alpha f_\alpha \mathrm{d}S \tag{8}$$

3. Spectral finite element formulation

3.1. Element matrices in plane stress

Let us apply the finite element method methodology to Eq. (8). The domain B of functional (8) is approximated as a sum $B \approx \bigcup_{e \in N_e} B_{(e)}$ where N_e is the number of finite elements. A typical finite element $B_{(e)}$ is defined as a smooth image of the so-called standard element $\pi_{(e)}$. In two-dimensional problem $\pi_{(e)} = [-1,+1]\times[-1,+1]$ is the element in the parent (natural) domain $\boldsymbol{\xi} = (\xi^1, \xi^2)$. It is assumed that the element has $N = m_1 \cdot m_2$ nodes where m_1 denotes the number of nodes in ξ_1 direction whereas m_2 in ξ_2 direction. To interpolate the variables, we use Lagrange type interpolation polynomials, with well-known properties, cf. e.g. [13]. The matrix of C^0 interpolation functions of the a-th node is $\underset{(2\times 2)}{\mathbf{L}_a(\boldsymbol{\xi})} = L_a(\boldsymbol{\xi})\,\underset{(2\times 2)}{\mathbf{I}}$ whereas the matrix of the whole N-node element (e) is

$$\mathbf{L}_{(e)}(\boldsymbol{\xi}) = [\mathbf{L}_1(\boldsymbol{\xi})\ \ \mathbf{L}_2(\boldsymbol{\xi})\ \ \ldots\ \ \mathbf{L}_N(\boldsymbol{\xi})] \tag{9}$$

Therefore the C^0 interpolation scheme for the typical vector variable of the problem is

$$\mathbf{u}(\boldsymbol{\xi},t) = \mathbf{L}_{(e)}(\boldsymbol{\xi})\,\boldsymbol{u}_{(e)}(t),\ \boldsymbol{u}_{(e)}(t) = \{\boldsymbol{u}_1(t), \boldsymbol{u}_2(t), \ldots, \boldsymbol{u}_N(t)\}^T,\ \boldsymbol{u}_a(t) = \{u_1(t), u_2(t)\}_a^T,\ a = 1,2,\ldots N \tag{10}$$

The time parameter in (10) is omitted when necessary for variables independent of time. Following usual methodology, the strain tensor (1) and its virtual counterpart are rewritten as vectors. In plane stress case this yields

$$\boldsymbol{\varepsilon} \to \boldsymbol{\varepsilon} = \begin{Bmatrix} \varepsilon_{11} \\ \varepsilon_{22} \\ 2\varepsilon_{12} \end{Bmatrix} = \boldsymbol{D}\mathbf{u}\,,\ \delta\boldsymbol{\varepsilon} \to \delta\boldsymbol{\varepsilon} = \begin{Bmatrix} \delta\varepsilon_{11} \\ \delta\varepsilon_{22} \\ 2\delta\varepsilon_{12} \end{Bmatrix} = \boldsymbol{D}\mathbf{w}\,, \quad \boldsymbol{D} = \begin{bmatrix} (.)_{,1} & 0 \\ 0 & (.)_{,2} \\ (.)_{,2} & (.)_{,1} \end{bmatrix} \tag{11}$$

The interpolation schemes then become

$$\boldsymbol{\varepsilon}(\xi,t) = \boldsymbol{D}\mathbf{L}_{(e)}(\boldsymbol{\xi})\,\boldsymbol{u}_{(e)}(t) = \mathbf{B}_{(e)}(\boldsymbol{\xi})\,\boldsymbol{u}_{(e)}(t)\,, \quad \delta\boldsymbol{\varepsilon}(\boldsymbol{\xi}) = \boldsymbol{D}\mathbf{L}_{(e)}(\boldsymbol{\xi})\boldsymbol{w}_{(e)} = \mathbf{B}_{(e)}(\boldsymbol{\xi})\boldsymbol{w}_{(e)} \tag{12}$$

where $\mathbf{B}_{(e)}(\boldsymbol{\xi}) = \boldsymbol{D}\mathbf{L}_{(e)}(\boldsymbol{\xi})$. The constitutive equation (2) may be written as

$$\begin{bmatrix} \sigma_{11} \\ \sigma_{22} \\ \sigma_{12} \end{bmatrix} = \frac{E}{1-\nu^2}\begin{bmatrix} 1 & \nu & 0 \\ \nu & 1 & 0 \\ 0 & 0 & \frac{1}{2}(1-\nu) \end{bmatrix}\begin{bmatrix} \varepsilon_{11} \\ \varepsilon_{22} \\ 2\varepsilon_{12} \end{bmatrix}, \quad \boldsymbol{\sigma} = \mathbf{E}\boldsymbol{\varepsilon} \tag{13}$$

Assuming that h_0 (the thickness of the panel) and ρ are constant over the element and in the light of the arbitrariness of $\boldsymbol{w}(\boldsymbol{\xi})$ and with representation (10) of all the vector variables of the problem, from (8) we obtain at the element level classical formulae

$$\int_B C_{\alpha\beta\gamma\pi} w_{(\alpha,\beta)} u_{(\gamma,\pi)} \mathrm{d}V \ \to\ \mathbf{K}_{(e)} = h_0 \int_B \mathbf{B}^T_{(e)}(\boldsymbol{\xi})\mathbf{E}\mathbf{B}_{(e)}(\boldsymbol{\xi})\,\mathrm{d}x_1\mathrm{d}x_2 \tag{14}$$

$$\int_B \rho w_\alpha\, \ddot{u}_\alpha \mathrm{d}V \ \to\ \mathbf{M}_{(e)} = \rho h_0 \int_B \mathbf{L}^T_{(e)}(\boldsymbol{\xi})\mathbf{L}_{(e)}(\boldsymbol{\xi})\,\mathrm{d}x_1\mathrm{d}x_2 \tag{15}$$

$$\int_B w_\alpha\, b_\alpha\, \mathrm{d}V + \int_{\partial B_f} w_\alpha\, f_\alpha \mathrm{d}S \ \to\ \mathbf{f}^{\mathrm{ext}}_{(e)} = h_0 \int_B \mathbf{L}^T_{(e)}(\boldsymbol{\xi})\,\boldsymbol{b}\,\mathrm{d}x_1\mathrm{d}x_2 + \int_{\partial B_f} \mathbf{L}^T_{(e)}(\boldsymbol{\xi})\,\boldsymbol{f}\,\mathrm{d}S \tag{16}$$

The Jacobian determinant $j(\boldsymbol{\xi}) = \det(\partial \boldsymbol{x}/\partial\boldsymbol{\xi})$ is

$$j(\boldsymbol{\xi}) = \frac{\partial x_1}{\partial \xi^1}\frac{\partial x_2}{\partial \xi^2} - \frac{\partial x_1}{\partial \xi^2}\frac{\partial x_2}{\partial \xi^1} \tag{17}$$

and the transformation formula for area element is $dV = h_0 dx_1 dx_2 = h_0\, j(\boldsymbol{\xi}) d\xi^1 d\xi^2$. The external load vector $\mathbf{f}^{\mathrm{ext}}_{(e)}$ (16) is supplemented with the vector of forces applied at element nodes i.e.

$$\mathbf{f}_{(e)} = \mathbf{f}^{\mathrm{ext}}_{(e)} + \mathbf{f}^{\mathrm{nod}}_{(e)}\,, \quad \mathbf{f}^{\mathrm{nod}}_{(e)} = \begin{Bmatrix} \boldsymbol{P}_1 \\ \vdots \\ \boldsymbol{P}_N \end{Bmatrix},\ \boldsymbol{P}_a = \begin{Bmatrix} P_{x1} \\ P_{x2} \end{Bmatrix}_a \tag{18}$$

where P_{x1}, P_{x2}, analogously to $\mathbf{f}^{\mathrm{ext}}_{(e)}$, are the components referred to global coordinate system.

The element matrices and load vectors (14)-(16) are integrated numerically. In general such integration is written as

$$\int_A \mathbf{g}(\boldsymbol{x})\mathrm{d}A \approx \sum_{p=1}^{M} \mathbf{g}\big(\boldsymbol{x}(\boldsymbol{\xi}_p)\big) w_p\, j(\boldsymbol{\xi}_p) \tag{19}$$

where it is assumed that the integrand $\mathbf{g}(\boldsymbol{x})$ is smooth and integrable for the integrals (8) and (14) -(16) to make sense. In (19) M denotes the number of integration points $p \in 1,2,\ldots,M$, $\boldsymbol{\xi}_p = (\xi^1, \xi^2)_p$ are the coordinates of integration point and $w_p = w_{\xi^1_p} w_{\xi^2_p}$ designates the associated weight. In the spectral element method, numerical integration is performed by Gauss-Lobatto-Legendre quadrature rule instead of Gauss-Legendre quadrature typically used

in classical FEM. In the employed GLL quadrature (cf. for instance [23], [24]) the coordinates of integration points coincide with element nodes and they satisfy the equation

$$(1-\xi^2)\frac{dP^{M-1}(\xi)}{d\xi}=0\,,\qquad M\leftarrow m_1,m_2 \tag{20}$$

whereas the weights follow from

$$w=\frac{2}{M(M-1)(P^{M-1}(\xi))^2}\,,\qquad M\leftarrow m_1,m_2 \tag{21}$$

where P^M denotes the M–th order Legendre polynomial defined as

$$P^M(\xi)=\frac{1}{2^M M!}\frac{d^M}{d\xi^M}[(\xi^2-1)^M]\,,\ \xi\leftarrow\xi^1,\xi^2 \tag{22}$$

Although the number of integration points is the same as the number of element nodes, the GLL integration rule used here cannot be termed ‘full integration’ since it can easily be checked that the mass matrix is underintegrated. In the literature, to the best our knowledge, the notions of full (FI) or reduced integrations (RI) for Lobatto rule are not so clear as they are for Gauss integration rule. For instance Pozrikidis in his book [25] introduced the notions of exact and inexact integration. He stated that the inexact integration by the Gauss-Lobatto-Legendre quadrature effectively diagonalizes the mass matrix by implementing mass lumping for any polynomial order.

As a consequence of properties of the shape functions and provided that the integration points $\boldsymbol{\xi}_p=(\xi^1,\xi^2)_p$ coincide with element nodes $\boldsymbol{\xi}_a=(\xi^1,\xi^2)_a$ the element mass matrix $\mathbf{M}_{(e)}$ in spectral element formulation is diagonal. The element stiffness $\mathbf{K}_{(e)}$ matrix, which is of full structure in general case, is not used directly in the present dynamic analysis. Instead, the dynamic equilibrium equations are written in terms of the vectors of inertia forces and internal forces defined respectively as

$$\mathbf{b}_{(e)}=\mathbf{M}_{(e)}\ddot{\mathbf{u}}_{(e)}\,,\quad \mathbf{r}_{(e)}=h_0\int_B\mathbf{B}^T_{(e)}(\boldsymbol{\xi})\boldsymbol{\sigma}_{(e)}(\boldsymbol{\xi})\,\mathrm{d}x_1\mathrm{d}x_2 \tag{23}$$

Global equations of motion are obtained in the course of standard aggregation procedure i.e.

$$\mathbf{M}=A_{e=1}^{N_e}\mathbf{M}_{(e)}\,, \tag{24}$$

$$\mathbf{p}=A_{e=1}^{N_e}\mathbf{f}_{(e)}\,,\quad \mathbf{b}=A_{e=1}^{N_e}\mathbf{b}_{(e)}\,,\quad \mathbf{r}=A_{e=1}^{N_e}\mathbf{r}_{(e)} \tag{25}$$

and the semi-discrete matrix counterpart of (8) becomes

$$\mathbf{M}\ddot{\mathbf{q}}=\mathbf{p}-\mathbf{r}(\mathbf{q}) \tag{26}$$

Here $\mathbf{q}$, $\ddot{\mathbf{q}}$ are vectors of displacements and accelerations, respectively. The temporal approximation of dynamic equilibrium equations (26) takes the advantage of the diagonal structure of matrices. This will be discussed in the next section.

3.2. Temporal approximation

Following standard argumentation, cf. of instance [13], the solution of linear equation of motion (26) is approximated $\mathbf{q}_n\equiv\mathbf{q}(t_n)$ in finite number of time points $t_1,t_2,...,t_n,....$, where

$t_i < t_{i+1}$. Assuming that $\mathbf{q}_n$ and $\ddot{\mathbf{q}}_n$ are known from the previous step, the solution at the next point $t_{n+1}=t_n+\Delta t$ is predicted as

$$\mathbf{M}\ddot{\mathbf{q}}_{n+1} = \mathbf{p}_{n+1} - \mathbf{r}(\mathbf{q}_{n+1}) \tag{27}$$

where Δt is the time step. The presence of $\mathbf{q}_{n+1}$ on rhs of (27) makes it an implicit scheme that requires iteration. Assuming Newmark's approximations [26] in iterative notation

$$\ddot{\mathbf{q}}_{n+1}^{(i+1)} = \ddot{\mathbf{q}}_{n+1}^{(i)} + \delta\ddot{\mathbf{q}} \tag{28}$$

$$\dot{\mathbf{q}}_{n+1}^{(i+1)} = \underbrace{\dot{\mathbf{q}}_n + \Delta t[(1-\gamma)\ddot{\mathbf{q}}_n + \gamma\ddot{\mathbf{q}}_{n+1}^{(i)}]}_{\dot{\mathbf{q}}_{n+1}^{(i)}} + \Delta t\gamma\delta\ddot{\mathbf{q}} = \dot{\mathbf{q}}_{n+1}^{(i)} + \Delta t\gamma\delta\ddot{\mathbf{q}} \tag{29}$$

$$\mathbf{q}_{n+1}^{(i+1)} = \underbrace{\mathbf{q}_n + \Delta t\dot{\mathbf{q}}_n + \tfrac{1}{2}(\Delta t)^2[(1-2\beta)\ddot{\mathbf{q}}_n + 2\beta\ddot{\mathbf{q}}_{n+1}^{(i)}]}_{\mathbf{q}_{n+1}^{(i)}} + (\Delta t)^2\beta\delta\ddot{\mathbf{q}} = \mathbf{q}_{n+1}^{(i)} + (\Delta t)^2\beta\delta\ddot{\mathbf{q}} \tag{30}$$

and substituting the above equations into (27), constitutes an implicit equation wrt iteration correction $\delta\ddot{\mathbf{q}}$

$$\mathbf{M}\delta\ddot{\mathbf{q}} = \mathbf{p}_{n+1} - \mathbf{b}_{n+1}^{(i)} - \mathbf{r}(\mathbf{q}_{n+1}^{(i)} + (\Delta t)^2\beta\delta\ddot{\mathbf{q}}) \tag{31}$$

Equation (31) is solved using simple iteration method leading to

$$\delta\ddot{\mathbf{q}} = \mathbf{M}^{-1}\left(\mathbf{p}_{n+1} - \mathbf{b}_{n+1}^{(i)} - \mathbf{r}(\mathbf{q}_{n+1}^{(i)})\right) \tag{32}$$

In view of the fact that $\mathbf{M}$ is diagonal, significant efficiency of time integration scheme is attained. Solution of (32) is then used to update the acceleration, velocity and displacement vectors through relations (28)-(30). The stability of the temporal integration scheme is determined by an appropriate choice of time step and parameters β and γ. Here $\beta=1/4$ and $\gamma=1/2$ which constitutes the average acceleration method.

The presented time integration scheme belongs to the GN22 group of algorithms (GN*pj* generalized Newmark [26] with degree $p=2$ and order $j=2$, see [27]). The algorithm inherits all the convergence properties of this group. The scheme described above is the closest to $\alpha-$ method predictor-corrector-iteration with the numerical damping coefficient (see [28]), here $\alpha=0$, since we are interested in propagation of fast wave phenomena. In comparison with the latter reference, in our case the effective mass matrix $\mathbf{M}+\Delta t\gamma\mathbf{C}$ is diagonal because it does not include participation of the stiffness matrix, and the residual value $\mathbf{j}_{n+1}^{(i+1)}$ comprises the vector $\mathbf{r}(\mathbf{q}_{n+1}^{(i+1)})$ treated as an implicit element. Therefore, we do not have to compute and store the element stiffness matrix, which even for a single multi-node element is very large and its computation and further processing are time consuming, see [9].

4. Tests of spectral elements

In all simulations in this paper the odd number of nodes per element side has been chosen. Thereby, there always exists one node in the middle of the element side. In addition, the element

nodes are always placed in accordance with Gauss-Lobatto-Legendre distribution as specified by (22) i.e. the moving of nodes is not allowed.

In addition, bearing in mind the focus of the paper, total energy density is computed pointwise. This formally requires projection of variables from integration points to nodes. Here, since the integration points coincide with element nodes, the nodal energy density is evaluated straightforwardly.

4.1. Cook's membrane problem

Before proceeding with dynamic analysis, we run three examples concerned with statics, to make sure that the formulated element is free of the locking effect, does not possess spurious zero-energy modes and is not sensitive to mesh distortion in the considered range of distortion in this study.

As the first example we run the well-known example of Cook's membrane problem (Fig .1), see e.g. [29], [33], [34]. We present our results of linear convergence analysis for displacement of point (a). Additionally, we report the Jacobian matrix and its determinant computed at points P1, P2, P3, P4 of the mesh. From the Table 1 it is seen that even though the elements are distorted, the obtained results of displacement are correct. In connection with *h*-convergence analysis for 11x11-node elements, the values exhibit typical growth with the refinement of mesh.

4.2. Simply supported beam

Considering however that in the Cook's membrane problem we deal with clamped edge, we run another example of simply supported beam, see Fig. 2. Thereby we are able to detect any spurious forms. The parameters are: L = 1 m, b = 5 cm, h = 12.5 cm, E = 200 GPa, $\nu = 0$, ρ = 7850 kg/m^3, P=100 kN. We have carried out *p*-convergence analysis of vertical displacement δ_A, as well as first three eigenfrequencies. The mesh density is 4 elements along beam's height and 32 along its length. The results are reported below in tables: for 4-node elements in Table 2, for 9-node elements in Table 3, for 25-node elements with GLL nodes in Table 4.

The above results show that with the growth of the order of polynomials the locking effect visible for 2x2 node elements disappear. In addition, we did not observe the spurious forms in deformations (Fig. 3). Moreover, even though the quadrature rule does not satisfy the necessary conditions required to fully integrate element matrices, the zero-energy modes did not appear in eigenfrequencies (we did not detect zero values). It is seen that the presented GLL integration rule is not exact (not to be mistaken with full integration). In the same time the scheme cannot be termed 'reduced integration' in the sense known from Gauss quadrature rule.

4.3. Cantilever beam, mesh distortion test, statics

Consider a mesh as shown in Fig. 4. In this test a beam undergoes bending with two plane stress elements in the mesh. The mesh distortion is controlled by scalar parameter Δ. The material parameters are $E = 1500$, $\nu = 0.25$. The units are [N] and [m]. The example is quite popular in the context of verification of low-order elements, see for instance [33], [34] [35], [36].

In the present example the following elements are taken into account: 3×3, 7×7 and 11×11 with GLL nodes. In comparison with original supporting conditions (shown in Fig. 4), here the vertical support has been placed at node C. Thereby it is possible to assess whether the

asymmetry of the beam response in horizontal direction is maintained. For the present elements two values of vertical displacements v_A and v_B (see Fig. 4) are reported in Table 5. The obtained results are compared with reference solutions in Table 5 where: Q1 denotes the standard bilinear quadrilateral element with Gauss integration, Q1/E4 is the enhanced assumed strain element [35], and PS is the hybrid stress element of Pian and Sumihara [33]. The exact solution is found using Bernoulli beam theory. From Table 5 it is seen that the present elements are almost insensitive to assumed mesh distortion. The higher order elements capture the local deformation at nodes of load placement, see Fig. 5. The deformation in this Figure is scaled by a factor 0.05.

4.4. Cantilever beam, mesh distortion test, dynamics

In this section we investigate the dispersion phenomenon induced by mesh distortion. In is known, see for instance [30] that in the analysis of the wave propagation, the effective length of the finite element, and the corresponding time step must be able to represent accurately the travelling wave. This requirement is known as the CFL condition, see for instance [5], [30], [31]. The values of CFL are also investigated here. The detailed consideration of the required node-to-node distances with respect to the wavelength is discussed in [32].

Consider a plane stress structure as shown in Fig 6 (dimensions are given in meters), made of steel for which we assume the values of: modulus of elasticity $E = 205$ GPa, mass density $\rho = 7850$ kg/m^3 and Poisson ratio $v = 0.25$. The structure is treated as free from boundary conditions and is acted upon by a single time dependent point force, placed at point (a) of assumed time variation in form of four-cycle sinusoidal wave of frequency 120 kHz modulated by the Hanning window (Fig. 7).

As in the previous example mesh distortion in controlled by the scalar parameter Δ. The CFL condition is written as

$$CFL = \frac{dt \cdot c_1}{h_{\min}} \tag{33}$$

where $dt = 5 \cdot 10^{-8}$ is the time step used for the calculation, $c_1 = 5277.84$ m/s is the velocity given by $(5)_1$ and $h_{\min}$ is the smallest distance between nodes.

Following [37] by varying the values of Δ we evaluate the dispersion denoted as c_h / c_1 where c_h is the numerically computed value of velocity c_1, recorded at point (b) in Fig. 6. The obtained values of CFL and the dispersion curve are plotted against Δ in Fig. 8. Judging from the graph of c_h / c_1 it is seen that the error is of order of 1%. As far as CFL is concerned its values grow with Δ however they are far below to the stability limit 1.0, see for example [38].

5. Applications

5.1. L-shaped panel with sharp corner

In the forthcoming computations we use spectral elements with 11×11 GLL nodes. Consider L-shaped panel in plane stress as shown in Fig. 9. The following material constants are

assumed in the analysis: modulus of elasticity $E = 205$ GPa, mass density $\rho = 7850$ kg/m^3 and Poisson ratio $v = 0.25$. The thickness of the structure is 5 mm. The structure is acted upon by the uniformly distributed reference load, applied at every FE node between points 1 and 2 in horizontal direction (Fig. 9). Time variation of load is given in Fig.7. The nodal values of reference load are computed according to (16). The structure is analysed as free. The time step used is $dt = 5 \cdot 10^{-8}$ s.

Bearing in mind future applications of the discussed formulation, the structure is discretized using elements with only two edges parallel (mesh A), though, in the analysis of the structure like this, a mesh composed of rectangular (square) elements seems an obvious choice (mesh B). The overall response of the structure with mesh A, expressed by energy history is plotted in Fig. 10. Since the differences between the results obtained with mesh A and B are very small we plot in Fig. 11 the relative error of potential (Fig. 11a) and kinetic (Fig. 11b) energy computed as

$$error = \frac{\text{result in mesh A} - \text{result in mesh B}}{\text{result in mesh A}} \tag{34}$$

Judging from these graphs, there is no qualitative difference between the responses of the structure. It may be also observed from Fig. 10 that during the simulation time span, the time integration scheme preserves the total energy of the system. The quantitative differences can be inspected in Table 6, where energies of the structure are given for $t = 1 \cdot 10^{-3}$ s. As it may be noted the computed value of load energy and value of summed internal and kinetic energy are equal and do not depend on the choice of the mesh. This fact provides strong evidence that the proposed time integration scheme is correct. In addition, Table 7 reports vector variable, that is horizontal and vertical accelerations of point (a) at $t = 1 \cdot 10^{-3}$ s.

In further analysis, we study the values of energy density at three selected points (see Fig. 9). By this it is meant that the total energy computed at selected point at given time instance is divided by the value of the total energy of the structure (Table 6, at $t = 1 \cdot 10^{-3}$ s.), divided by the volume of the panel. Thereby, it is possible to evaluate the amount of energy of waves that travel perpendicularly i.e. in the vertical arm of the structure. Fig. 12a depicts the comparison of results obtained for point (a), Fig. 12b for point (b) and Fig. 12c for point (c). The respective graphs show no difference between values obtained in different meshes. It is seen that point (a) receives about 40 % of the total energy carried by the propagating waves and overall motion of the whole structure while points (b) and (c) only about 20 %.

5.2. L-shaped panel with a stiffener

Consider an L-shaped panel with a triangle stiffener located at the right-hand angle, see Fig. 13. The material properties and time integration step are the same as in the previous example. The load is the same as in the previous case. Fig 14 depicts the energy conservation for the system. As in previous case the total energy of the structure is preserved.

In the analysis to follow we concentrate on comparison between results obtained in mesh A and in mesh C. Again energy plots are used, this time however due to the different volumes of

structure A and C, we compare total energy density at selected point without normalization. Fig. 15a shows the results for point (a), Fig. 15b for point (b) and Fig. 15c for point (c). While the results obtained in point (a) have comparable peak values, the analysis of solutions computed in point (b) reveals highest peak values in mesh C. The largest differences between results are pronounced in point (c).

To throw some light on this issue we have selected 11 points between nodes (c) and (d) at equal distance of 0.2 m. In each selected point we have plotted the total energy variation over simulation time. Fig. 16a shows the results in the mesh A, and Fig 16b for the mesh C. In both plots the vertical axis denotes the height of the horizontal arm of the L-structure. It may be observed that in point (d) $(h = 0)$ the graphs are the almost the same. With the growth of y coordinate the computed energy plots attain their maximal values for $y \approx h/2 = 0.1$ m and results are comparable between mesh A and mesh C. Finally, on the upper edge of the panel for $y = h$ in point (c) we note the largest discrepancies between the results obtained in mesh A and mesh C. This is due to the fact that this point is located in the place where the width of the panel changes. The analysis of Fig. 16 shows that the greatest part of the energy is carried by the motion of the middle part $y \approx h/2$ of the panel.

6. Conclusions

In this paper, properties of spectral elements in statics and dynamics test were investigated. The present paper is concentrated on numerical tests. However, the developed code can be used for wave propagation simulations in a reference state of a structure. Such numerical model can be intended as a part of the structural health monitoring system utilizing non-destructive guided wave propagation technique.

The presented formulation and the numerical results support the following conclusions

1) The elements' matrices are integrated numerically with GLL quadrature rule, in which number of integration point equals the number of element nodes. Locking effect and spurious zero-energy forms have not been observed. These undesired effects may appear in low order elements available in commercial codes with explicit time integration scheme.
2) The formulated higher order spectral finite elements perform well in distorted meshes.
3) Since the elaborated temporal integration scheme is not designed to conserve the energy of the structure, it is proposed to verify the selection of time step by controlling the total energy of the system. Within the studied simulation times the algorithm worked out here preserves the total energy.
4) Studying the energy values shows that the relatively small portion of energy propagates through right-hand angle joint. This should serve as the guidance in the aspect of potential damage detection by using waveguides. This problem will be the subject of the future studies.

Acknowledgements

This work was partially supported by the project POIG 01.01.02-10-106/09.

References

[1] T. Patera, A spectral element method for fluid dynamics: laminar flow in a channel expansion, Journal of Computational Physics, 54 (1984), 468–488.

[2] J. F. Semblat, J. J. Brioist, Efficiency of higher order finite elements for the analysis of seismic wave propagation, Journal of Sound and Vibration, 231(2) (2000) 460–467.

[3] P. Moczo, J. Kristek, M. Galis, E. Chaljub, V. Etienne, 3-D finite-difference, finite-element, discontinuous-Galerkin and spectral-element schemes analysed for their accuracy with respect to P-wave to S-wave speed ratio, Geophys. J. Int. (2011) 187, 1645–1667.

[4] S. Chaillat, M. Bonnet, J-F. Semblat, A multi-level fast multipole BEM for 3-D elastodynamics in the frequency domain, Comput. Methods Appl. Mech. Engrg. 197 (2008) 4233–4249.

[5] E. Faccioli, F. Maggio, R. Paolucci, A. Quarteroni, 2D and 3D elastic wave propagation by a pseudospectral domain decomposition method, Journal of Seismology, 1, 237–251, 1997.

[6] D. Komatitsch, R. Martin, J. Tromp, M.A. Taylor, B.A. Wingate, Wave propagation in 2-D elastic media using a spectral element method with triangles and quadrangles, Journal of Computational Acoustics, 9 (2001), 703–718.

[7] Y. Liu, N.Hu, C.Yan, X.Peng, B.Yan, Construction of a Mindlin pseudospectral plate element and evaluating efficiency of the element, Finite Elements in Analysis and Design 45 (2009) 538–546

[8] J. Chróścielewski, M. Rucka, W. Witkowski, K. Wilde, Formulation of spectral truss element for guided waves damage detection in spatial steel trusses. Archives of Civil Engineering, LV(1) (2009), 43–63.

[9] W. Witkowski, M. Rucka, J. Chróścielewski, K. Wilde, Wave propagation analysis in spatial frames using spectral Timoshenko beam elements in the context of damage detection. Archives of Civil Engineering, LV(3) (2009), 367–402.

[10] P. Kudela, A. Żak, M. Krawczuk, W. Ostachowicz, Modelling of wave propagation in composite plates using the time domain spectral element method. Journal of Sound and Vibration, 302 (2007), 728–745.

[11] R. Sridhar, A. Chakraborty, S. Gopalakrishnan, Wave propagation analysis in anisotropic and inhomogeneous uncracked and cracked structures using pseudospectral finite element method. International Journal of Solids and Structures, 43 (2006), 4997–5031.

[12] A. Żak, M. Krawczuk, Certain numerical issues of wave propagation modelling in rods by the Spectral Finite Element Method. Finite Elements in Analysis and Design 47 (2011), 1036–1046.

[13] T.J.R. Hughes, The Finite Element Method: linear static and dynamics finite element analysis. Dover Publications, Inc., New York, 2000.

[14] J.E. Marsden, T.J.R. Hughes, Mathematical foundations of elasticity, Dover Publications, Inc., New York, 1994.

[15] G.W. Benthien, M.E. Gurtin, T.D. Ralston, On the semi-discrete Galerkin method for hyperbolic problems and its application to problems in elastodynamics, Archive for Rational Mechanics and Analysis, 48 (1972), 51–63.

[16] L.D. Landau, E.M. Lifshitz. Theory of Elasticity, third edition, Butterworth-Heinemann, 2000.

[17] C.A. Truesdell, General and exact theory of waves in finite elastic strain, Archive for Rational Mechanics and Analysis, 8 (1961), 263–296.

[18] J.C. Simo, N. Tarnow. The discrete energy–momentum method. conserving algorithms for nonlinear elastodynamics, ZAMP 43 (1992), 757–793.

[19] I. Romero, F. Armero, An objective finite element approximation of the kinematics of geometrically exact rods and its use in the formulation of an energy-momentum conserving scheme, Int. J. Numer. Meth. Eng. 54 (2002), 1683–1716.

[20] J. Chróścielewski, I. Lubowiecka, W. Witkowski, Dynamics based on six-field theory of shells in the context of energy-conserving scheme. Shell structures: Theory and applications / eds. Wojciech Pietraszkiewicz, Czesław Szymczak, London: Taylor & Francis/Balkema, 2005. - (Proceedings and Monographs in Engineering, Water and Earth Sciences), pp. 303-307, Proceedings of the 8th SSTA Conference. Jurata, Poland, 12-14 October 2005.

[21] L. Vu-Quoc, X.G. Tan, Optimal solid shells for non-linear analyses of multilayer composites. II. Dynamics. Comput. Methods Appl. Mech. Engrg. 192 (2003), 1017–1059.

[22] D. Braess, Finite elements. Theory, fast solvers and applications in solid mechanics. Cambridge University Press, 2007.

[23] M. Abramovitz, I.A. Stegun, Handbook of mathematical functions with formulas, graphs, and mathematical tables. United States Department Of Commerce, National Bureau Of Standards, 1970.

[24] F.B. Hildebrandt, Introduction to numerical analysis. McGraw-Hill Book Company Inc. 1956.

[25] C. Pozrikidis, Introduction to Finite and Spectral Element Methods using MATLAB®. Chapman & Hall/CRC, 2005

[26] N.N. Newmark, A method of computation for structural dynamics. Proc. ASCE, J. Engng. Mech. Div. 85 (1959) (EM3).

[27] O.C. Zienkiewicz, R.L. Taylor, The Finite Element Method, Butterworth-Heinemann, 2000.

[28] I. Miranda, Ferencz R.M., T.J.R. Hughes, An improved implicit-explicit time integration method for structural dynamics, Earthquake Eng. Struct. Dyn. 18 (1989), 643–655.

[29] R.D. Cook, Improved two dimensional finite element. J. Struct. Div. ASCE, 100 (1976), 1851–1863.

[30] K.J. Bathe.: Finite Element Procedures. Upper Saddle River, New Jersey: Prentice Hall 1996.

[31] T. Lähivaara, M. Malinen, J. P. Kaipio, T. Huttunen, Computational aspects of the discontinuous galerkin method for the wave equation, Journal of Computational Acoustics, Vol. 16, No. 4 (2008) 507–530

[32] M. Rucka, Experimental and numerical studies of guided wave damage detection in bars with structural discontinuities. Archive of Applied Mechanics 80: 1371–1390, 2010

[33] T.H.H. Pian, K. Sumihara, Rational approach for assumed stress finite elements, Int. J. Num. Meth. Engng, 20 (1984), 1685–1695.

[34] R. Piltner, R.L. Taylor, A systematic construction of B-bar functions for linear and non-linear mixed-enhanced finite elements. UCB/SEMM Report 96/02, University of California at Berkeley, 1996.

[35] J.C. Simo, M.S. Rifai. A class of mixed assumed strain methods and the methods of incompatible modes, Int. J. Num. Meth. Engng, 29 (1990), 1595–1638.

[36] K. Wisniewski, E. Turska, Improved 4-node Hu–Washizu elements based on skew coordinates, Computers and Structures 87 (2009) 407–424.

[37] G. Cohen, S. Fauqueux, Mixed finite elements with mass-lumping for the transient wave equation, Journal of Computational Acoustics, Vol. 8, No. 1 (2000) 171-188.

[38] D. Lax, R. D. Richtmyer, Survey of the stability of linear finite difference equations, Communications On Pure And Applied Mathematics, vol. IX, 267-293 (1956).

Tables

Table 1. Results for Cook's membrane: displacements, Jacobian matrix and determinant of Jacobian matrix

Mesh	$u_{(a)}$	$v_{(a)}$	Jacobian, determinant DET
10×10 (2×2)node el. 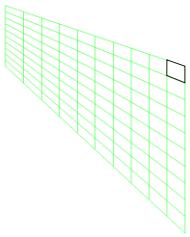	1.00399E+01	2.26940E+01	P1: $J=\begin{bmatrix}2.4 & -2.17041\\ 0 & 0.829585\end{bmatrix}$, $\det J = 1.9910052$
			P2: $J=\begin{bmatrix}2.4 & -0.829585\\ 0 & 0.829585\end{bmatrix}$, $\det J = 1.9910052$
			P3: $J=\begin{bmatrix}2.4 & -2.17041\\ 0 & 2.17041\end{bmatrix}$, $\det J = 5.2089948$
			P4: $J=\begin{bmatrix}2.4 & -0.829585\\ 0 & 2.17041\end{bmatrix}$, $\det J = 5.2089948$
1 (11×11)node el. 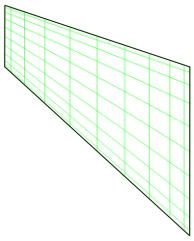	1.06826E+01	2.39414E+01	P1: $J=\begin{bmatrix}24 & -22\\ 0 & 8\end{bmatrix}$, $\det J = 192$
			P2: $J=\begin{bmatrix}24 & -8\\ 0 & 8\end{bmatrix}$, $\det J = 192$
			P3: $J=\begin{bmatrix}24 & -22\\ 0 & 22\end{bmatrix}$, $\det J = 528$
			P4: $J=\begin{bmatrix}24 & -8\\ 0 & 22\end{bmatrix}$, $\det J = 528$
2×2 (11×11)node el. 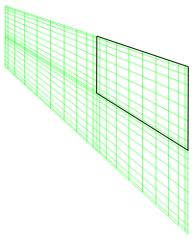	1.06893E+01	2.39554E+01	P1: $J=\begin{bmatrix}12 & -11\\ 0 & 4\end{bmatrix}$, $\det J = 48$
			P2: $J=\begin{bmatrix}12 & -4\\ 0 & 4\end{bmatrix}$, $\det J = 48$
			P3: $J=\begin{bmatrix}12 & -11\\ 0 & 11\end{bmatrix}$, $\det J = 132$
			P4: $J=\begin{bmatrix}12 & -4\\ 0 & 11\end{bmatrix}$, $\det J = 132$
3×3 (11×11)node el. 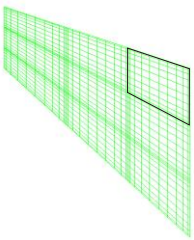	1.06910E+01	2.39581E+01	P1: $J=\begin{bmatrix}8 & -7.3(3)\\ 0 & 2.6(6)\end{bmatrix}$, $\det J = 21.3(3)$
			P2: $J=\begin{bmatrix}8 & -2.6(6)\\ 0 & 2.6(6)\end{bmatrix}$, $\det J = 21.3(3)$
			P3: $J=\begin{bmatrix}8 & -7.3(3)\\ 0 & 7.3(3)\end{bmatrix}$, $\det J = 58.6(6)$
			P4: $J=\begin{bmatrix}8 & -2.6(6)\\ 0 & 7.3(3)\end{bmatrix}$, $\det J = 58.6(6)$

Table 2. Results for simply supported beam (4-node elements): bending modes and displacements

	Analytical: Euler-Bernoulli beam	**FEM: Gauss FI**	**SEM: Gauss- Lobatto-Legendre**
δ_A [mm]	1.28	1.29113	1.09678
mode 1 [Hz]	286.1	284.36	308.17
mode 2 [Hz]	1144.4	1074.0	1154.9
mode 3 [Hz]	2574.9	2232.5	2377.6

Table 3. Results for simply supported beam (4-node elements): bending modes and displacements

	Analytical: Euler-Bernoulli beam	**FEM: Gauss FI**	**SEM: Gauss- Lobatto-Legendre**
δ_A [mm]	1.28	1.33912	1.33747
mode 1 [Hz]	286.1	279.10	279.26
mode 2 [Hz]	1144.4	1045.1	1047.2
mode 3 [Hz]	2574.9	2147.5	2155.9

Table 4. Results for simply supported beam (25-node elements with GLL nodes): bending modes and displacements

	Analytical: Euler-Bernoulli beam	**FEM: Gauss FI**	**SEM: Gauss- Lobatto-Legendre**
δ_A [mm]	1.28	1.34558	1.34462
mode 1 [Hz]	286.1	278.48	278.57
mode 2 [Hz]	1144.4	1036.9	1038.1
mode 3 [Hz]	2574.9	2113.6	2118.6

Table 5. Results of mesh distortion test for cantilever beam, results in [m]

Distortion Δ / *Element*		**0.0**	**0.5**	**1.0**	**2.0**	**3.0**	**4.0**	**4.9**
Exact solution		100	100	100	100	100	100	100
Q1 (FI)		28.037	21.047	14.129	9.707	8.305	7.204	6.243
Q1/E4		100.0	80.935	62.711	54.439	53.635	51.240	46.801
PS		100.0	81.0	62.9	55.0	54.7	53.1	49.8
3×3 GL/GLL NODES	v_A	100.250	100.250	100.250	100.250	100.250	100.250	100.250
	v_B	100.000	100.000	100.000	100.000	100.000	100.000	100.000
7×7 GLL NODES	v_A	101.496	101.440	101.386	101.283	101.190	101.104	101.043
	v_B	100.016	100.017	100.020	100.033	100.056	100.081	100.112
11×11 GLL NODES	v_A	102.432	102.361	102.294	102.173	102.064	101.967	101.883
	v_B	100.001	100.001	100.000	99.9983	99.9985	100.002	99.9863

Table 6. Energies of L-shaped panel, $t=1\cdot10^{-3}$ s.

	U [J]	K [J]	G_{ext} [J]	$U+K$ [J]
Mesh A	2.96157E–12	3.07037E–12	6.03193 E–12	6.03193E–12
Mesh B	2.96291E–12	3.06902E–12	6.03193 E–12	6.03193E–12

Table 7. Accelerations of point 5, $t=1\cdot10^{-3}$ s.

	Horizontal [m/s^2]	*Vertical* [m/s^2]
Mesh A	–2.61456E–01	6.23417E–01
Mesh B	–2.05386E–01	6.22643E–01

Figure captions

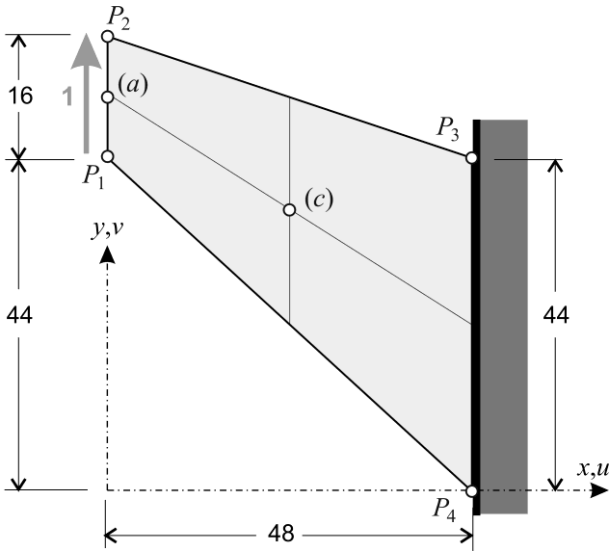

Fig. 1. Cook's membrane, geometry and load

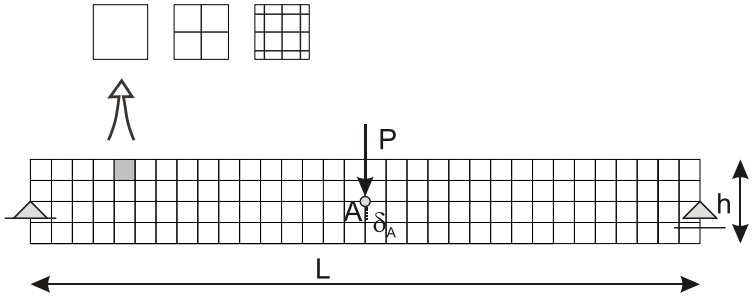

Fig. 2. Simply supported beam, geometry and load

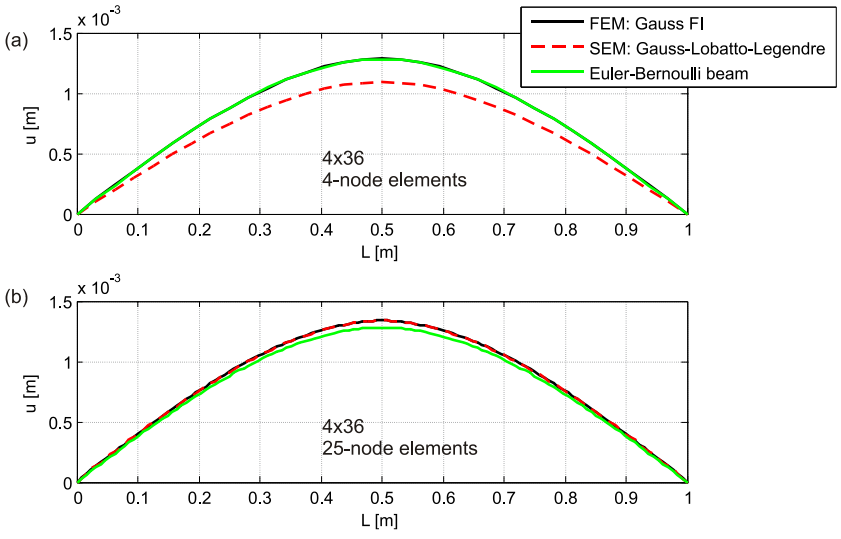

Fig. 3. Deflection of simply supported beam for mesh density 4 × 32 elements: a) 4-node elements; b) 25-node elements with GLL nodes

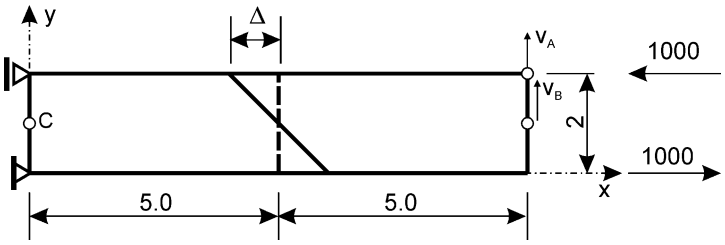

Fig. 4. Cantilever beam, geometry and load, statics

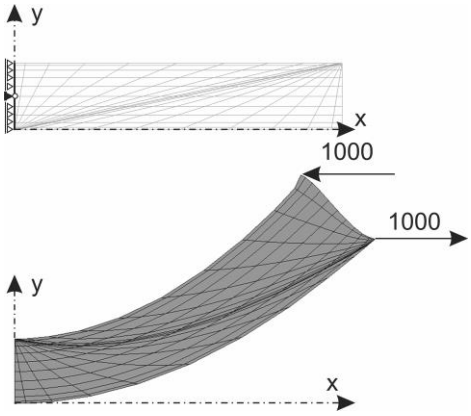

Fig. 5. Cantilever beam, statics, distortion Δ=4.9, 11×11 node element,

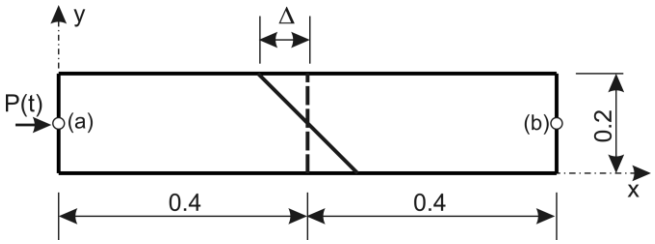

Fig. 6. Plane stress structure in dynamic analysis, dimensions in [m]

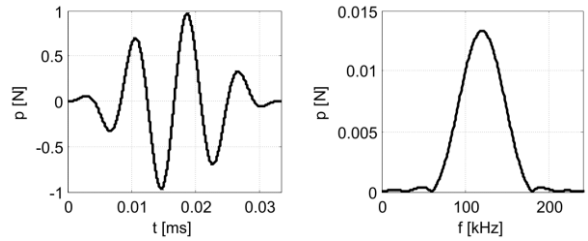

Fig. 7. An excitation signal in the time and frequency domains

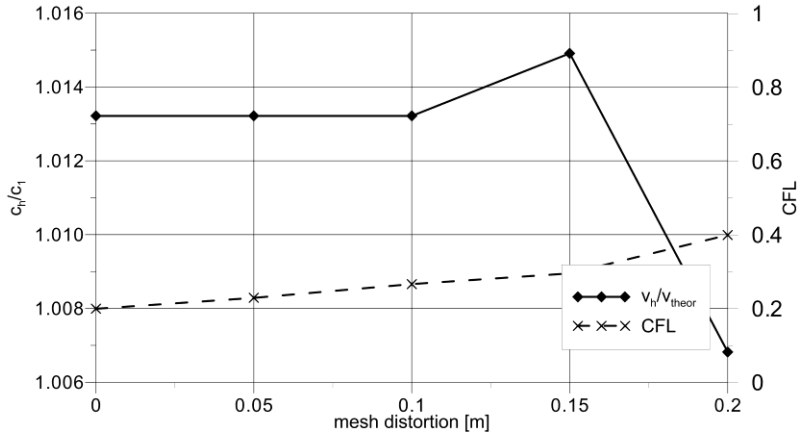

Fig. 8. Dispersion curve and CFL variation on mesh distortion parameter for plane stress structure in dynamic analysis, dimensions in [m]

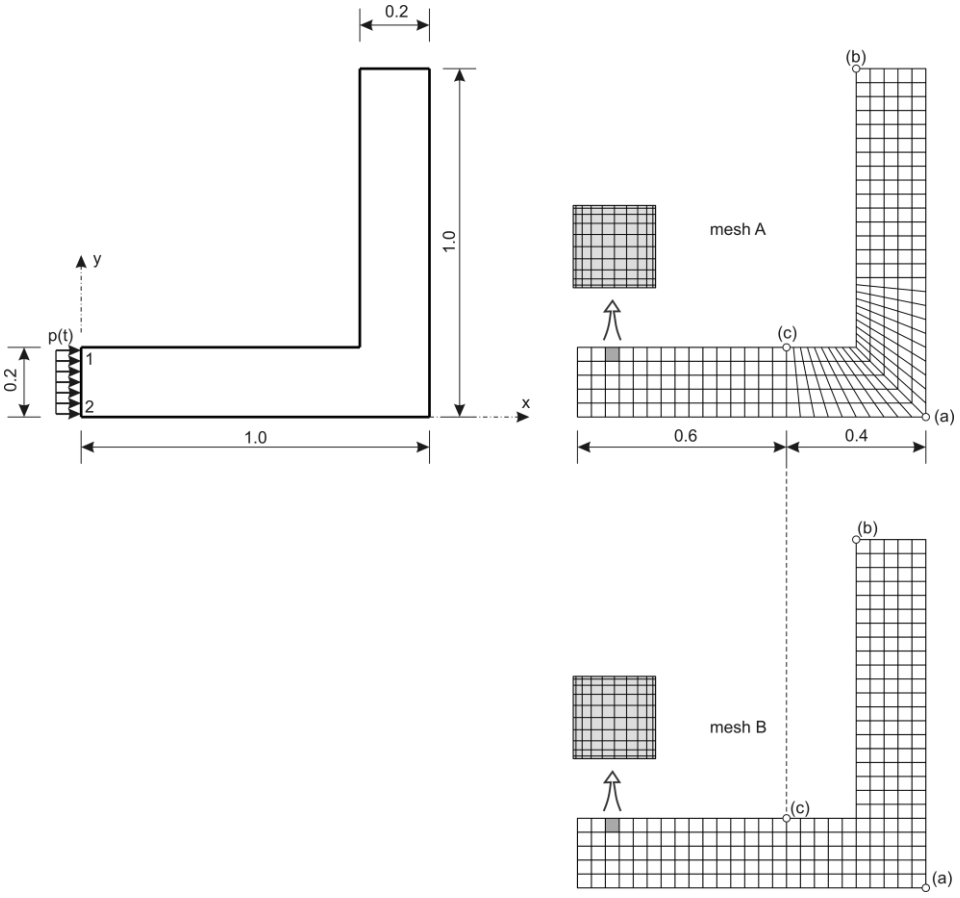

Fig. 9. L-shaped panel, geometry, load and applied meshes

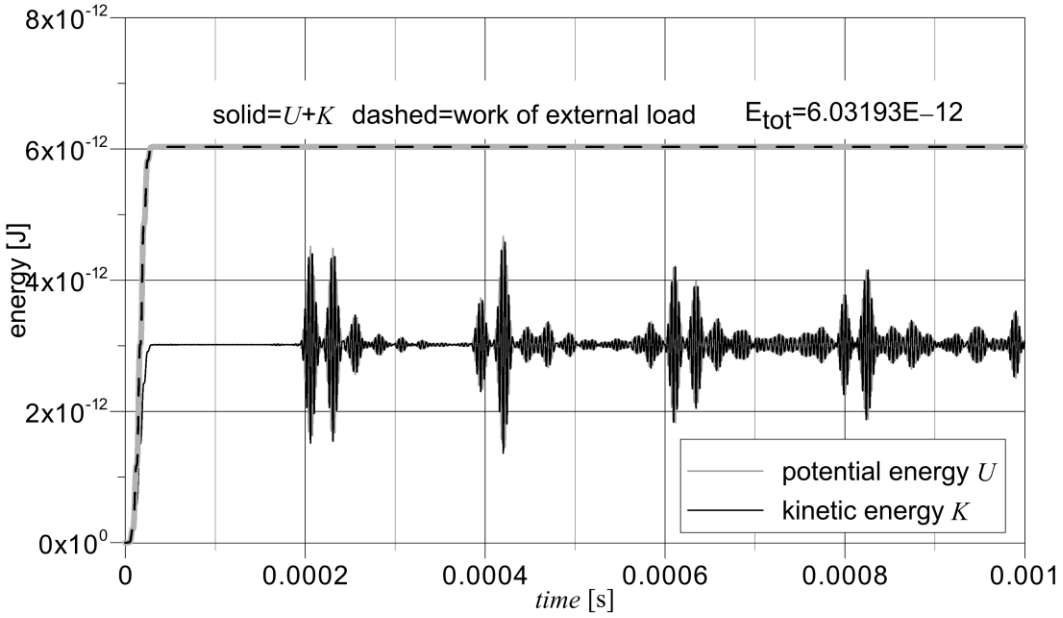

Fig. 10. Energy history of the L-shaped panel for mesh A

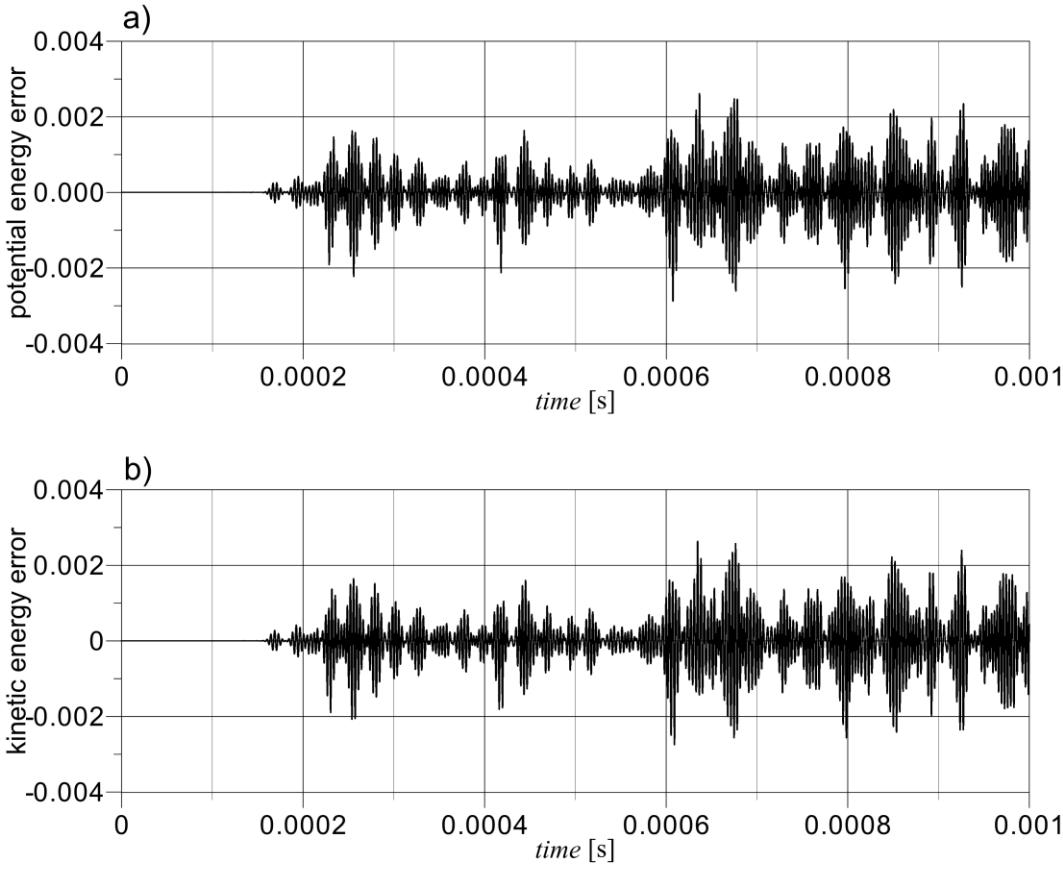

Fig. 11. Potential and kinetic energy error between mesh A and mesh B

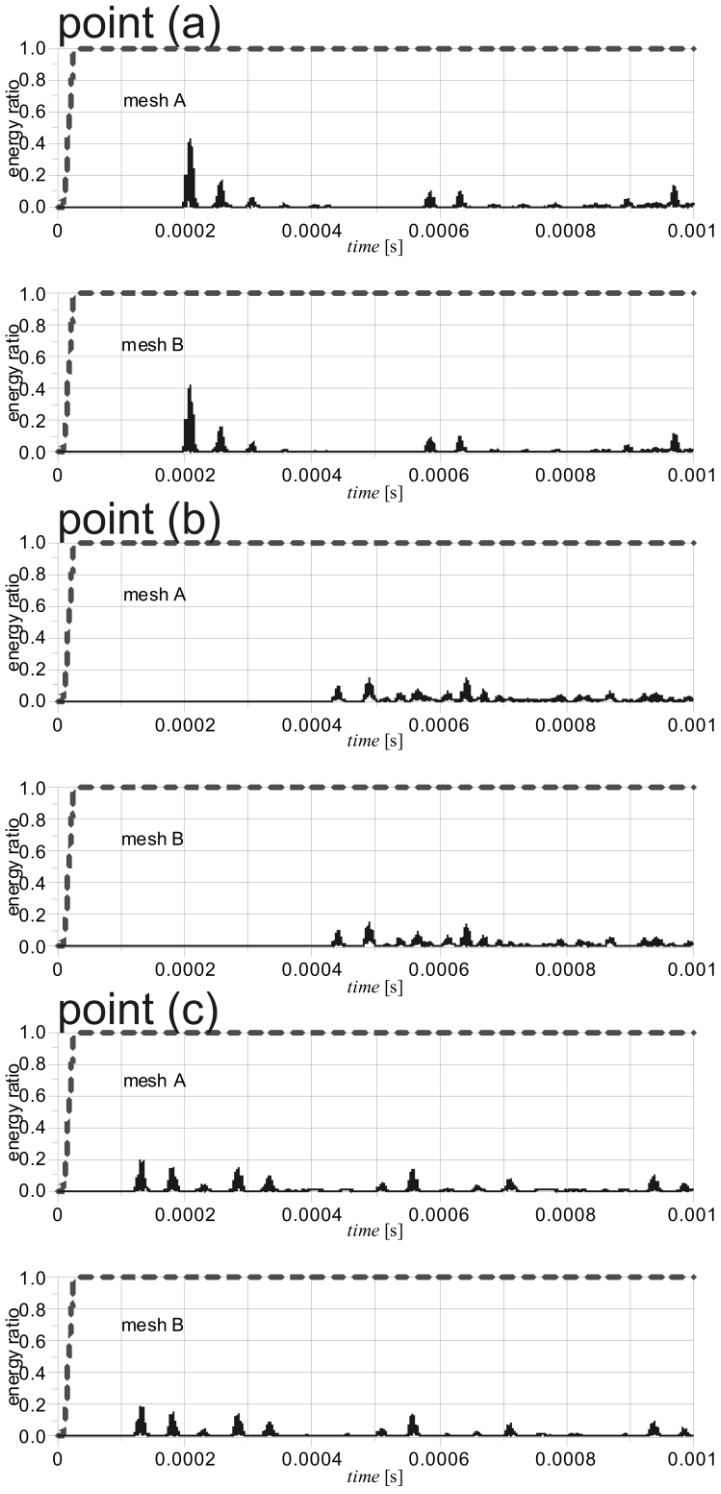

Fig 12. Energy ratio for the L-shaped panel for mesh A and mesh B in selected points:
a) point (a); b) point (b); c) point (c)

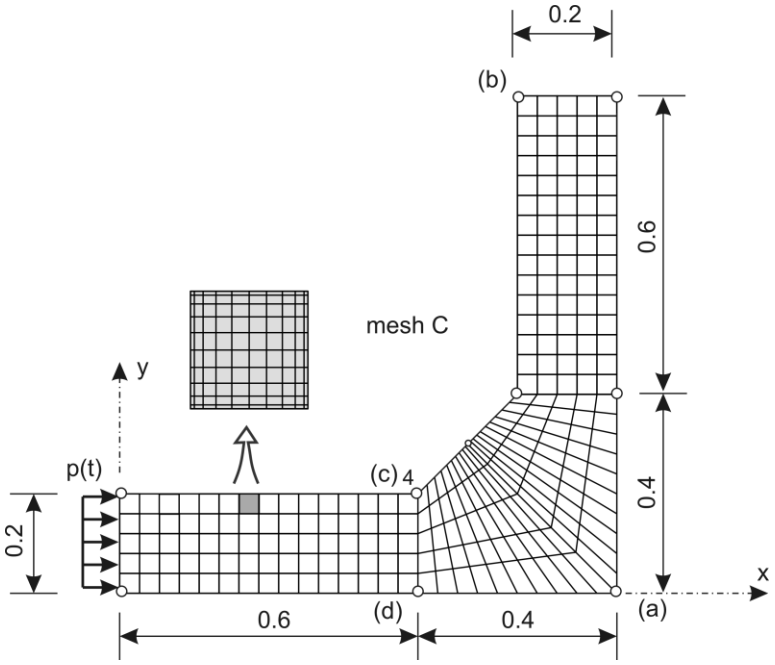

Fig. 13. L-shaped panel with stiffener, mesh C, geometry and load

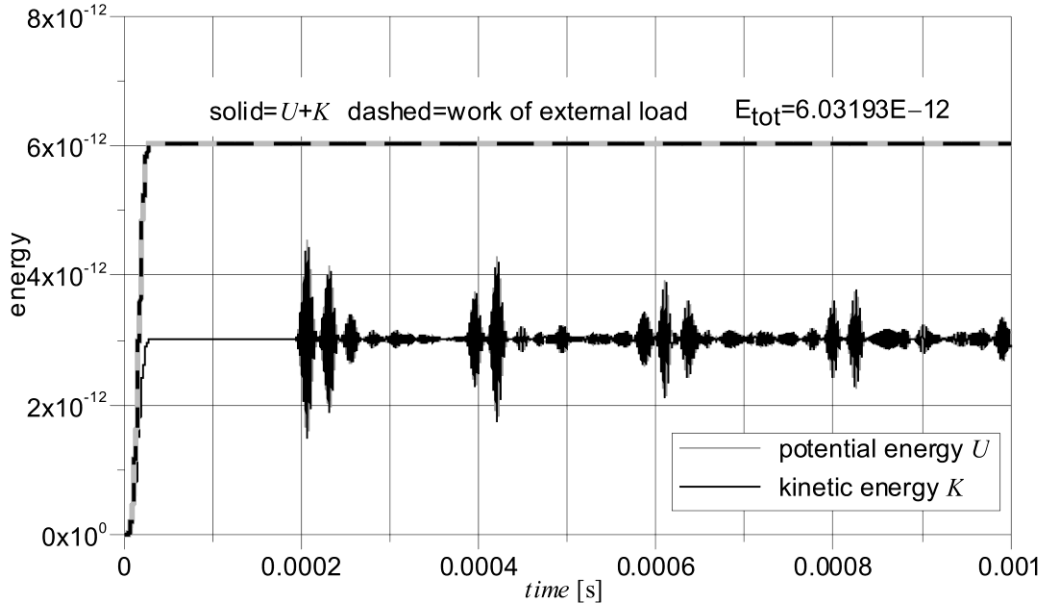

Fig. 14. Energy history for the L-shaped panel with stiffener for mesh C

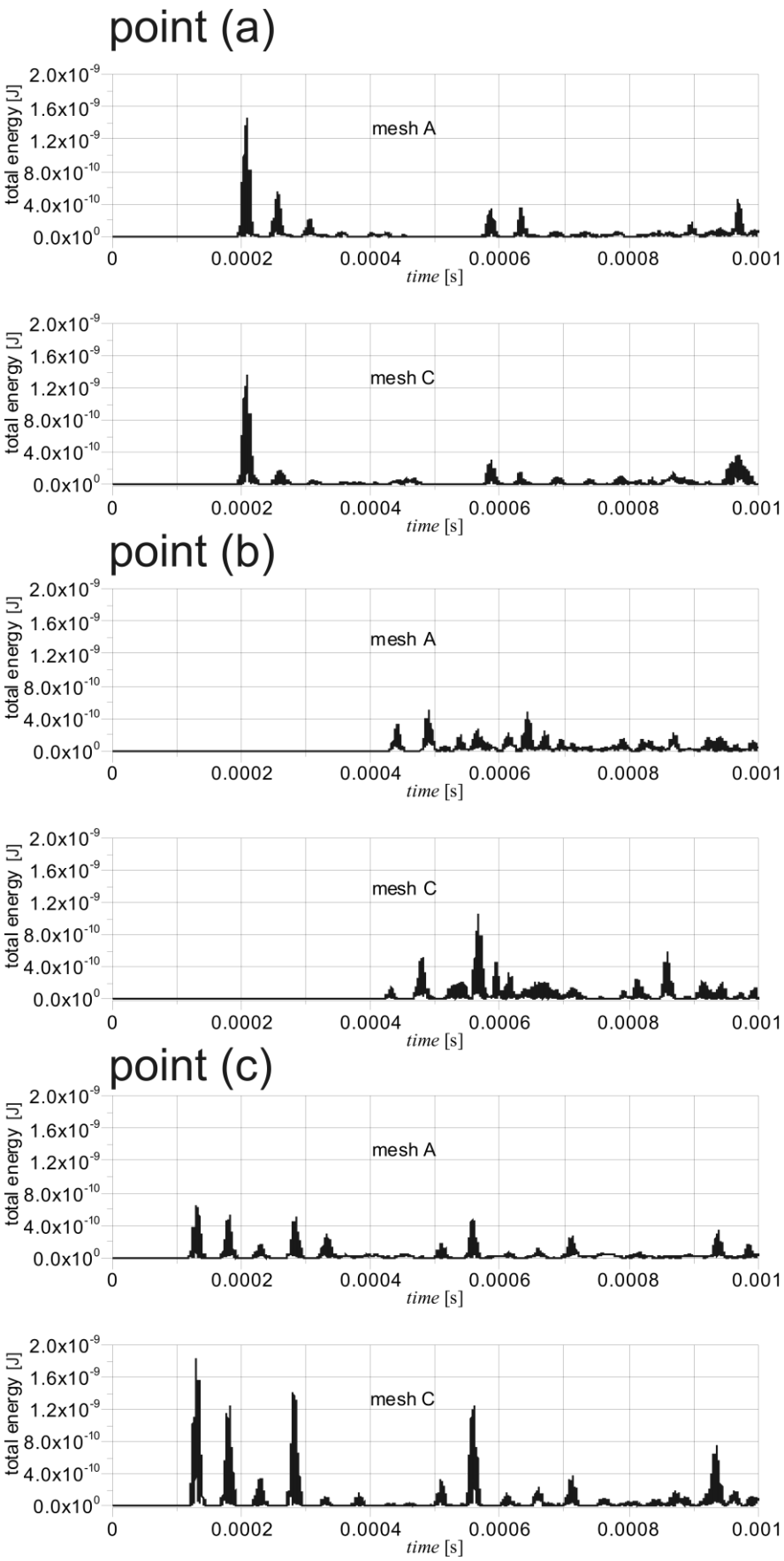

Fig 15. Energy for the L-shaped panel for mesh A and mesh C in selected points:
a) point (a); b) point (b); c) point (c)

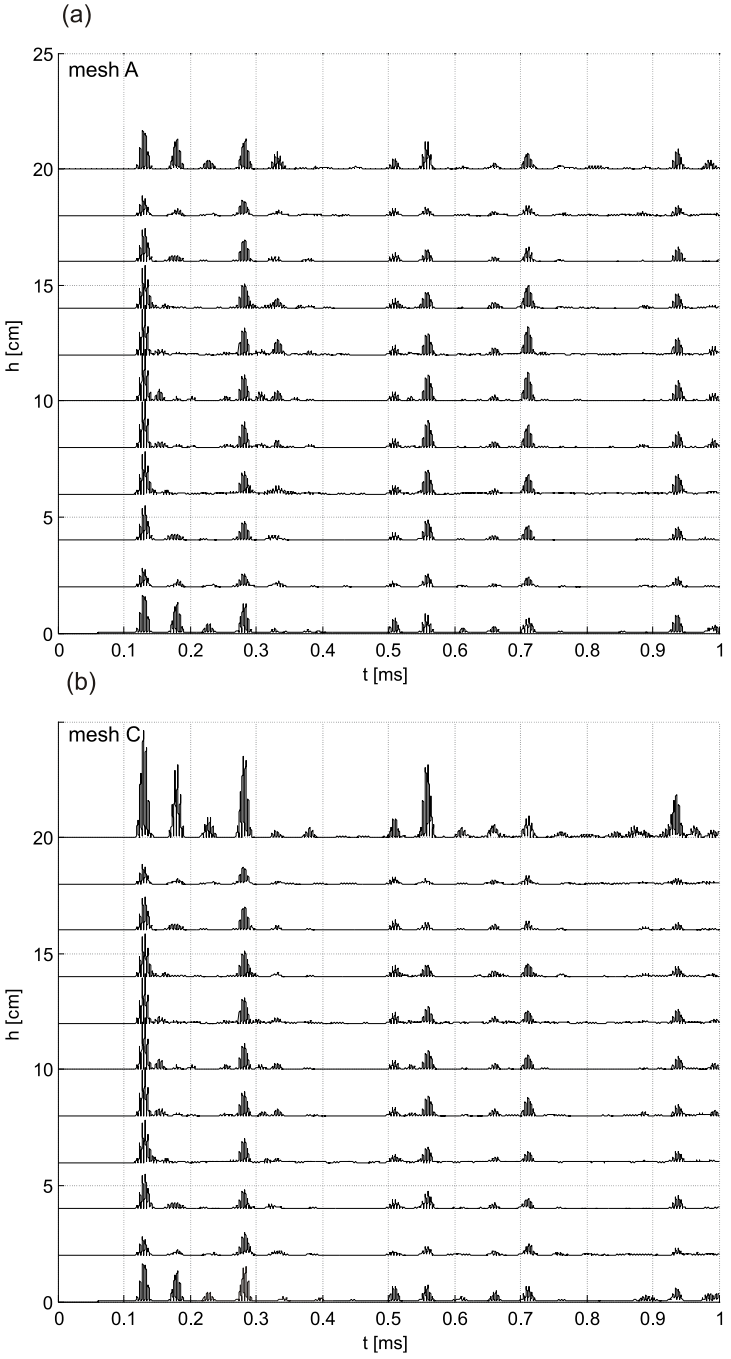

Fig. 16. Energy plots in L-shaped panel for points located between nodes (c) and (d): a) mesh A; b) mesh C